

Imaging, single atom contact and single atom manipulations at low temperature using the new ScientaOmicron LT-UHV-4 STM

Jianshu Yang¹, Delphine Sordes^{1,2}, Marek Kolmer³, David Martrou¹, and Christian Joachim^{1,4,a}

¹ Nanoscience Group & MANA Satellite, CEMES/CNRS, 29 rue Marvig, BP 94347, 31055 Toulouse Cedex, France

² CEATech Midi-Pyrénées, Campus INSA, Bât. GM 135 avenue de Rangueil, 31400 Toulouse, France

³ Centre for Nanometer-Scale Science and Advanced Materials, NANOSAM, Faculty of Physics, Astronomy and Applied Computer Science, Jagiellonian University, Lojasiewicza 11, 30-348 Krakow, Poland

⁴ International Center for Materials Nanoarchitectonics (MANA), National Institute for Materials Science (NIMS), 1-1 Namiki, Tsukuba, Ibaraki 305-0044, Japan

Received: 25 September 2015 / Received in final form: 8 December 2015 / Accepted: 21 December 2015
Published online: 15 January 2016 – © EDP Sciences 2016

Abstract. The performances of the new ScientaOmicron LT-UHV 4-STM microscope have been certified by a series of *state-of-art* STM experiments on an Au(111) surface at 4.3 K. During the STM operation of the 4 STM scanners (independently or in parallel with an inter tip apex front to front distance down to a few tens of nanometers), a ΔZ stability of about 2 pm per STM was demonstrated. With this LT-UHV 4-STM stability, single Au atom manipulation experiments were performed on Au(111) by recording the pulling, sliding and pushing manipulation signals per scanner. Jump to contact experiments lead to perfectly linear low voltage I - V characteristics on a contacted single Au ad-atom with no need of averaging successive I - V 's. Our results show how this new instrument is exactly 4 times a very precise single tip LT-UHV-STM. Two tips surface conductance measurements were performed on Au(111) using a lock-in technique in a floating sample mode of operation to capture the Au(111) surface states via two STM tips dI/dV characteristics.

1 Introduction

Low temperature scanning tunneling microscopes (LT-UHV-STM) are well known instruments. They are able to deliver atomic resolution images on ultra-high vacuum (UHV) atomically well prepared metal and semiconductor surfaces [1] with a vertical resolution (ΔZ) better than a few picometer for the best instruments [2]. Using the different parameters available on an STM (the tunnel current intensity I , the bias voltage V and the tip end apex surface distance Z), I - Z , I - V , dI/dV and dI/dZ characteristics can be recorded locally on the imaged surface or on a single adsorbate (atom, molecule). Single atom [3,4] and single molecule manipulations [5] can be performed on the more stable LT-UHV-STM instruments. It is also possible to record the $I(t)$ time dependent feedback current (the so-called manipulation signal) during an atomic scale manipulation to get the precise mechanical behavior of the adsorbate during its STM manipulation [6]. Because an STM is based on the scanning of a single atomically sharp metallic tip, it also offers a lot of possibilities in term of electronic transport measurements for example by approaching the tip apex

end atom in electronic contact atop an adsorbate [7–9], laterally [10] or by doing the reverse i.e., by pulling from one end the molecule out of its supporting surface [11–13].

To perform more advance atomic scale electronics and also single molecule mechanics experiments [14], a single metallic tip is not enough. This is for example the case for atomic scale transport measurements in a planar configuration on a surface [15], for transport measurements along dangling bond (DB) atomic wires atom by atom constructed on a passivated semi-conductor surface [16–19] and for molecule mechanics with the expected measurement of the motive power of a single molecule motor [20,21]. For example, a complete test of the functioning of the recent atom by atom constructed NOR/OR Boolean logic gate on Si(100)H [22] is demanding at least 4 atomic scale electrical access to this gate. On this DB circuit, each of the 2 inputs can be performed by a small molecular switch i.e., a single chemisorbed molecule whose end phenyl interacts (or not) in a butterfly configuration with the corresponding input DB dimer. The bi-stability of a given molecular switch input will be controlled by positioning the STM tip apex directly on the switchable phenyl group and its bias voltage pulsed. The output status measurement is performed using 2 STM tips

^a e-mail: joachim@cemes.fr

positioned at both end of short atomic scale DB wires interacting with the 3 DB dimers of the calculating block of the NOR/OR logic gate [22].

Driven by piezo motors, the first generation of UHV 4-probes systems have been around for quite some times [23–26]. But this first generation had not demonstrated reproducible atomic resolution per tip nor the nice possibilities of state-of-art LT-UHV-STM experiments like single atom manipulation. Very recently, the situation had changed with the new version of the low temperature UHV 4-probes released by ScientaOmicron where each STM scanner is truly a high performance LT-UHV-STM by itself as demonstrated here. Furthermore, the four LT-UHV-STM of this new 4-probes head (here after called LT-UHV 4-STM) can scan independently on the same surface under the tip navigation of a high resolution UHV-SEM microscope.

In this paper, we report the complete exploration of the performances of our LT-UHV 4-STM head recently delivered by ScientaOmicron. This new equipment was tested and tuned on an Au(111) surface. On this new instrument, we have basically reproduced per scanner all the STM experiments recalled above and performed since 20 years on the most stable single tip LT-UHV-STM. After a specific tuning to its vibrational environment, we demonstrate here how this new instrument is exactly 4 times a very precise LT-UHV-STM. The inter tip apex distance can go from millimeters to a few nanometer on the same surface depending on the tip apex end radius of curvature used during the measurements. We have performed imaging (Sect. 3), electronic measurements at atomic scale (Sects. 4 and 5) and achieved single atom manipulation as well (Sect. 6) using alternatively the 4 scanners available on our LT-UHV 4-STM. No difference in performances were noticed between them. Only the tip apex mounted of each scanner can differ from tip to tip. We demonstrate how this new LT-UHV 4-STM & UHV-SEM extends experimental capabilities of a 4-probes system down to atomic scale (Sect. 7 for 2 tip floating electrical measurements). All the presented measurements have been performed at 4.3 K.

2 The LT-UHV 4-STM

The new LT-UHV 4-STM was installed on a large static anti-vibration concrete block equipped with a passive anti-vibration legs system. It is the last version of the UHV 4-probes systems constructed by ScientaOmicron. Delivered in September 2014 to our Pico-Lab low noise clean-room building and running since February 2015, our new instrument has also its specific UHV sample and tip preparation chambers UHV interconnected to the LT-UHV 4-STM chamber. It is also equipped with a very specific UHV-transfer printing chamber [27] and with specific miniature molecular evaporators to allow multiple molecular species sublimation. In this paper, we only focused on the LT-UHV 4-STM head of our system which is the new part as compared to its first version described in reference [25]. Our head has 4 independent miniature

LT-UHV-STM scanners able to scan on the same surface and in parallel.

The sample must be mounted on a standard ScientaOmicron UHV transfer plate. This transfer plate can circulate from place to place in our UHV system depending on the sequence of operations from the introduction to the UHV chamber to imaging, atom manipulation and atomic scale electronic contacting. Since all the imaging, manipulations and electrical measurements are performed directly under the LT-UHV 4-STM head, there is no need on our new system for a specific and long LT transfer between the chambers as it was the case on the previous version of this equipment [25]. As illustrated by the Figure 1a photo of our LT-UHV 4-STM stage, a very convenient 28 positions carousel is servicing the LT-UHV 4-STM head where the tip holders, the sample plates and for example a miniature molecular evaporators can be stored. The LT-UHV 4-STM stage is shielded by 2 thermal radiation shields in contact with respectively LN2 and LHe cryostats. The transfer of a sample plate in the cryostat is performed during the opening of a very convenient double doors system through the shields (not shown in Fig. 1a). The head hosts both the sample stage and the four tips holders with their respective piezo drivers, called hereafter PS1, PS2, PS3 and PS4. The stage is attached to the cryostat and to extra cooling wires introduced to the LT-UHV 4-STM stage house as well. This guarantees both sample stage and the 4 tips with their piezo scanners to be working at the same temperature. The working temperature can be selected to be 4.3 K, 78 K or room temperature with a possible heating to go step by step from 4.3 K to 78 K and so on.

The sample stage can be translated in X and Y directions by specific piezo motors over a range of about 3 mm in each direction. A Zeiss UHV SEM Gemini column electron microscope with a resolution of 15 nm is mounted atop the LT-UHV 4-STM head to monitor the tips position and when necessary to image micro and mesoscale objects. The end of the SEM gun is positioned at the center of the LT-UHV 4-STM head (see Figs. 1b and 4 for a better view of a 4 scanning tips configuration UHV SEM imaged). It is better to lock the sample stage for SEM scanning operations and to release it during STM operations. In this case, the LT-UHV 4-STM head is supported by mechanical springs damped by a magnetic system. After its release, a few hours are required to reach the best performance of each of the 4 LT-UHV-STM scanners.

For the LT-UHV 4-STM head itself, each scanner accommodates a specific tip holder and its piezo scanner. Each scanner is controlled by one matrix electronic controller unit independent of the others. The maximum scanning range for each scanner is about $2.0 \mu\text{m}$ at 4.3 K with no apparent deformation of the STM image recorded at least up to $1.6 \mu\text{m}$ as presented in Figure 2 for PS3. We have taken a specific care for the grounding of the LT-UHV 4-STM sample stage. Since the general design of this new LT-UHV 4-STM head originates from a 4 probes measurement problem at the nanoscale, the sample stage is grounded. We have added a specific very high

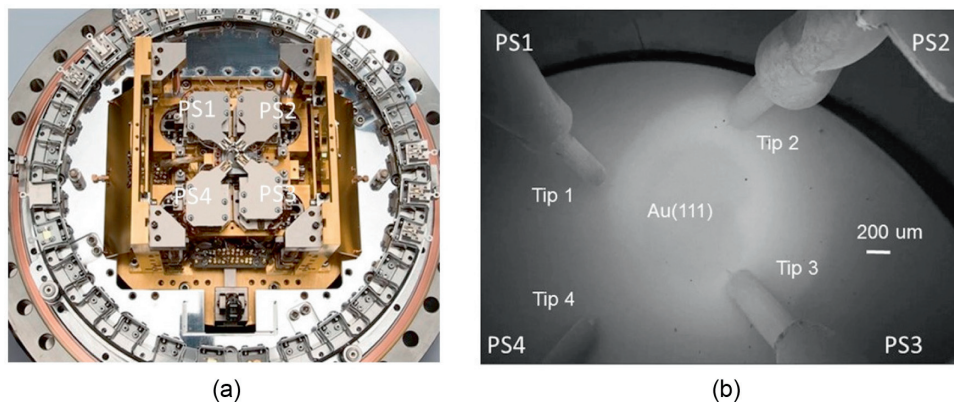


Fig. 1. (a) A top view optical photo of the LT-UHV 4-STM stage with all the cryostat shielding stage out. The SEM gun is coming also on top of this stage. The servicing carousel with 28 slots is clearly visible together with the four piezo scanners and their wiring. (b) While completely re-assembled, an SEM top view image showing the 4 tips, the tip holders and one part of piezo scanner PS2 (SEM image recorded at 5 kV, 400 pA with a magnification of 54).

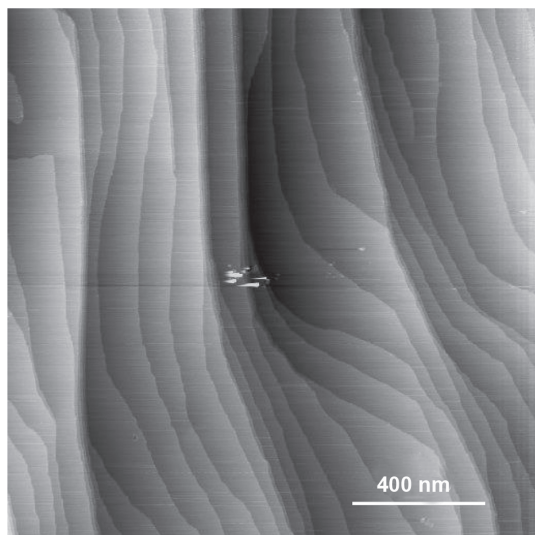


Fig. 2. A $1.6 \mu\text{m} \times 1.6 \mu\text{m}$ extra-large constant current STM image using piezo scanner PS3 of the Au(111) surface recorded at 300 pA for a 200 mV bias voltage. 34 mono-atomic step have been recorded on the imaged area with no double tip effect demonstrating that after a bit of re-construction a gold tip apex can be nicely stabilized at the tungsten facet of a 45° mounted tip. Notice the small impurity at the center of the image which was perturbed by the scanning.

independence electronically controllable relay to switch on and off the sample stage ground [15]. In that case, multiple tips electrical floating measurements are possible independent of each STM I - V converter (and of the matrix controllers) via also a specific electronic switch per tip. The range of the I - V converters is 0.0 to 3.3 nA (or 0.0 to 333 nA) for each scanner. After a good offset tuning per I - V converter, they all present the same sensitivity and noise level (see also Fig. 6).

When the ground of the sample stage is disconnected, STM imaging is only possible by using 2 STM tips, one for scanning and one used as a top counter electrode

connected directly to the ground or via the virtual ground of its I - V converter. Another consequence of the 4-prober origin of our new LT-UHV 4-STM, each tip holder is maintaining its tip 45° inclined relative to the sample surface and not vertically as in a standard single tip LT-UHV-STM (see Figs. 1b and 4). We have modified some tip holders to recover a 90° standard STM configuration. This offers a better stability for I - V measurements and for single adsorbate manipulations. From the top, a partial SEM view of each tip apex can still be recovered in this 90° case by performing a specific modification of the tip holder body.

3 Sample and tip preparations

On our LT-UHV 4-STM, sample and tip preparations are performed external to the cryostat and then loaded on the servicing carousel before being introduced on the LT-UHV 4-STM stage. For certifying our LT-UHV 4-STM, we have selected the Au(111) surface. The sample is a commercial single crystal Au(111) from MaTecK with only one side polished. After its introduction into the UHV preparation chamber attached to our LT-UHV 4-STM chamber, the sample surface was cleaned by Ar^+ sputtering with energy of 1 keV and a current of $5 \mu\text{A}$ for 10 min. Then, the Au(111) sample was annealed at 450°C for 20 min. After 3 cycles of sputtering and annealing, an atomically clean Au(111) surface was obtained. The Au(111) surface terraces and mono atomic steps can be imaged by each scanner, as shown in Figure 2. This image was recorded using PS3. The same images were also recorded using PS1, PS2 and PS4 when the tips loaded on those scanners are atomically well defined (see the discussion below). Two face to face 45° inclined tips can be approached in mutual contact according to the SEM image. One tip can even scan the tip end apex of the other one in a way to measure the tip to tip end apex distance (see Sect. 7 below).

To get the same STM images from all the scanners and in a 45° tip holder configuration, many tips must be

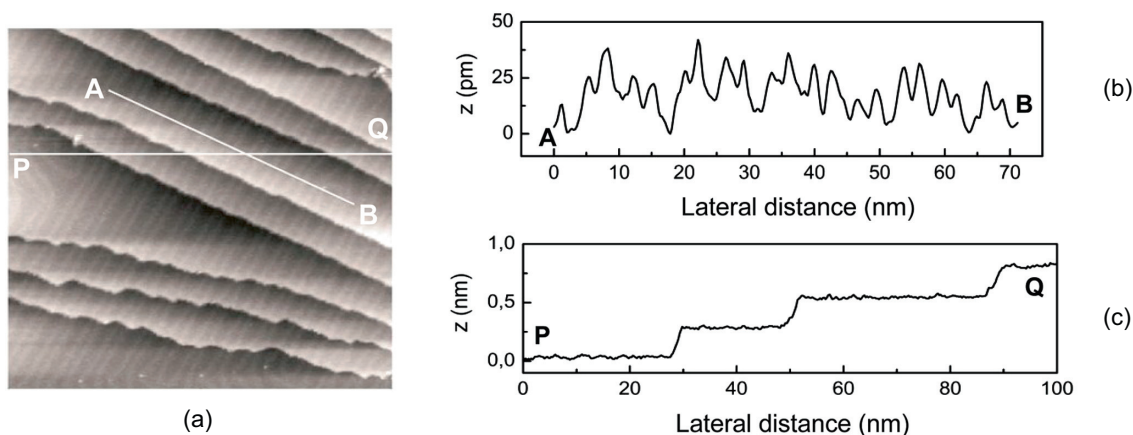


Fig. 3. (a) A 100 nm \times 100 nm constant current STM image using piezo scanner PS3 of the Au(111) surface recorded at 170 pA for a 100 mV bias voltage showing the native $(22 \times \sqrt{3})$ herringbone Au(111) surface structure on the terraces separated by the mono-atomic steps. These herringbones terminate at the $[2\ 1\ 1]$ mono atomic steps and extend continuously down to the neighbor lower terrace. (b) A constant current line scan crossing the herringbone structure on the same terrace from A to B in image (a). The hcp and bcc areas are arraying periodically along AB line alternatively. (c) A constant current line scan crossing the mono atomic 0.2 nm surface steps from P to Q.

tested as compared with a standard single tip LT-UHV-STM operation. When a tip is scanned in a 45° configuration, it is mainly its end facet and not its apex end atom which is forming the tunneling junction with the surface. This renders more delicate the usual tip forming procedure practiced in-situ on a standard LT-UHV-STM by applying large bias voltage pulses to reconstruct the tip end apex atomic structure. With a tip facet facing the sample surface, a bias voltage pulse can shape a few and almost equivalent atomic scale apex. In this case, a few tips must be tested per scanner to be able to shape the good one. Electrochemically etched tungsten tip have been loaded on the 45° tip holders as shown in SEM image Figures 1b and 4. Then, each tip has been in-situ re-prepared by a gentle mechanical indentation (8–10 Å in the Au(111) surface) together with a bias voltage pulse from +4 to +5 V. With this preparation technique, stable tip apex can be reconstructed even in a 45° configuration. As compared to a single tip LT-UHV-STM, more tips must be tested per scanner before getting a good one for scanning or for dI/dV spectroscopy. In this prospect, the servicing carousel presented in Figure 1a is very important for loading new tips. With our specific 90° tip holder, this problem doesn't occur. Here, we have recovered the normal tip re-construction procedure of a standard LT-UHV-STM. In our actual utilization of this new LT-UHV 4-STM head and since this head was designed for atomic scale contact, we have mainly worked up to now with three 45° and one 90° oriented tips.

4 Atomic resolution

Conditioned by the tip apex used per scanner, each piezo scanner was independently tested and is presenting the same scanning characteristics and performances. On the

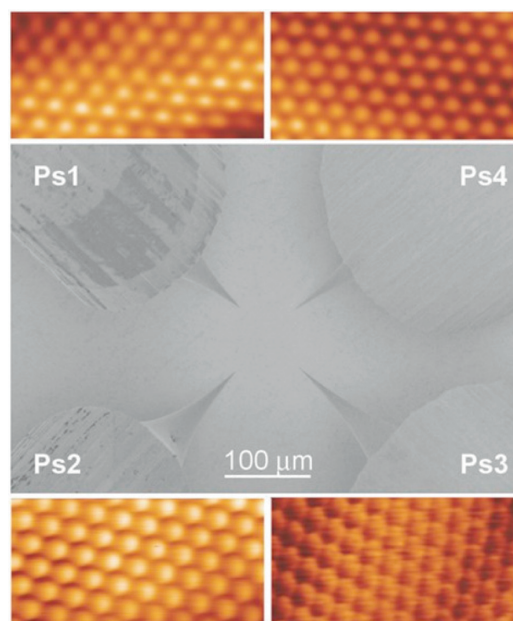


Fig. 4. Atomic resolution constant current STM images of Au(111)-(1 \times 1) surface recorded with the scanners PS1, PS2, PS3 and PS4 with in each case an optimized 45° oriented tip. The central SEM image is illustrating the position of each tip during the scanning. The size of all the STM images is 3 nm \times 1.5 nm recorded at 200 pA for a 500 mV bias voltage. Notice the difference in corrugation between each image indicating how the tip apex used are different per scanner. Those images can be recorded independently and in parallel (see also Fig. 14).

Au(111) atomically clean surface, the STM image recorded with PS3 is presented in Figure 3. The nice mono-atomic surface step series imaged in Figure 2 is

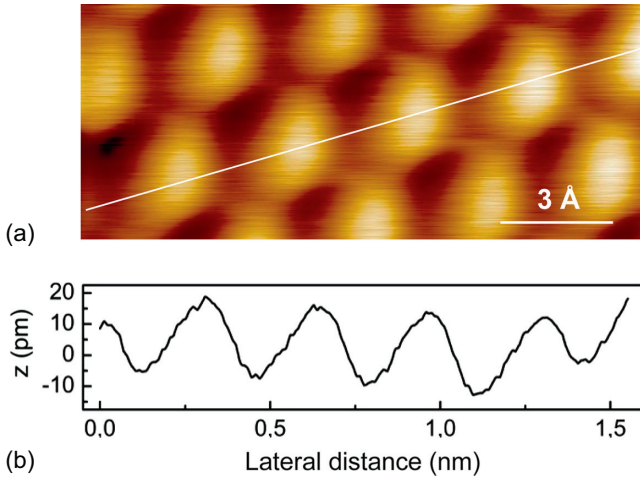


Fig. 5. (a) A $1.5 \text{ nm} \times 0.75 \text{ nm}$ zoom-in on the Figure 4 PS2 constant current image of the Au(111) (1×1) flat area recorded at 320 pA for a 50 mV bias voltage. As indicated on the extracted scan line (b), the apparent corrugation with those scanning conditions is $\Delta Z = 20 \text{ pm}$ with a noise level in ΔZ of about 2 pm. The surface inter atomic distance along the [110] direction is 2.9 \AA to be compared with the 2.885 \AA surface crystallographic distance.

recovered plus the herringbone structure of the $22 \times \sqrt{3}$ reconstructed terraces and the Au(111)-(1×1) surface atomic structure in between the reconstructions. In Figure 3, the herringbone structure are arraying with hcp and bcc areas following a period of 13.7 nm. The profile lines crossing the herringbone structure shows a surface corrugation corresponding to the crossing from fcc to hcp. Each herringbone structure is ending at a 0.2 nm mono atomic step height with the herringbone structure continuously extending on the neighbor lower terrace [28].

Each scanner being equipped with a 45° tip orientation and after a zoom-in on a flat Au(111)-(1×1) surface area, the PS1, PS2, PS3 and PS4 scanners are all able to deliver nice atomic scale resolution images as presented in Figure 4 with a bit of corrugation difference coming again from tip apex difference from scanner to scanner. Those images can be recorded in series or in parallel with no differences as soon as there is no mechanical interaction between the scanned tip apexes. At 4.3 K, the thermal drift recorded on each scanner is $<0.9 \text{ nm/h}$ in x -direction and $<0.02 \text{ nm/h}$ in y -direction on our system. The 1×1 atomic surface structure presented in Figure 4 is exhibiting the periods 3.1 \AA , 2.9 \AA and 2.79 \AA in the three surface sample $\{110\}$ directions. The error of 8.5% and -2.3% are caused by the inequivalent thermal drift in the X and Y scanning directions. For a 50 mV bias voltage and for a feedback current of 320 pA, the Au(111) (1×1) apparent surface atomic corrugation is 20 pm with a noise level of about 2 pm for example on PS2 (Fig. 5). This very good imaging performance (equivalently observed on the 4 scanners for the Au(111) surface) demonstrates how each LT-UHV-STM scanner of our LT-UHV 4-STM head is equivalent to a very stable single tip LT-UHV-STM head.

5 I-Z curves and jump to contact

Through vacuum and between a metallic tip and a metallic surface, the tunneling current intensity depends exponentially on the tip apex end atom to surface distance Z . It follows the well known $I = I_0 e^{-\beta z}$ decay law [29]. Here, $\beta = 2\sqrt{\frac{2m}{\hbar^2}}\phi$ is the tunneling inverse decay length through vacuum and in first approximation ϕ is the average work function between the 2 metals in action in the tunnel junction. Here, it is most certainly gold and gold in view of our tip apex preparation procedure on the Au(111) surface. Similar I - Z curves were recorded very early during the STM invention period [30]. Using PS1, we have reproduced the standard I - Z characteristics first in a retraction mode of operation in a way not to transform the tip apex end during the approach mode (see below). After selecting a nice atomically clean area on the Au(111) surface, away from a mono atomic step and for the same 10 mV bias voltage, 3 feedback tunneling current intensity values were selected: 20 nA, 2 nA and 200 pA to fix up the starting tip apex end atom height relative to the surface. Then, the feedback loop was switched off during 7 s. While retracting continuously in Z the tip mounted on PS1, the tunneling current intensity was recorded up to the limit of the I - V convertor functioning. The retraction time duration was 5 s. As presented in Figure 6, those three I - Z curves are perfectly matching from each other and when superposed, they are spanning more than 6 orders of magnitude in I . As expected, when the tip is retracted from the surface, the tunneling current intensity decreases exponentially. Using $\Phi = 0.95 \left(\frac{d(\ln I)}{dz} \right)^2$ and from Figure 6, an apparent barrier height of $3.43 \text{ eV} \pm 0.2 \text{ eV}$ is obtained instead of about 5 eV for a gold-gold vacuum tunnel junction. There are a few explanations for this difference. For example, the Z piezo variation may not be fully linear over those 6 orders of magnitude (the same for the I - V convertor) and the exact tip apex composition may not be exactly gold or fully metallic (see the next section). In any case, the Figure 6 reported measurements are demonstrating a nice functioning of the PS1 scanner and can be reproduced on all the 3 other scanners. In Figure 6, all the I - Z curves are saturating down when reaching about 0.9 pA. This is the actual noise limit of the I - V convertor connected to the tip mounted on PS1. It was about the same value for all the others I - V convertors. On Figure 6 and by expanding those curves up and towards a possible tip apex to Au(111) surface single atom electronic contact, one is reaching $I_0 = G_0 V$ at about $Z_0 - 2 \text{ \AA}$ with $V = 10 \text{ mV}$ where G_0 is one quantum of conductance (see below). Notice that the absolute Z_0 value is generally not known in STM. Its value was set up here using the 20 nA, 10 mV feedback conditions.

After recording the I - Z tunnel junction characteristics in a retraction mode and being satisfied by the excellent stability of the piezo scanners in Z of our LT-UHV 4-STM head (Fig. 6), we have also performed the reverse that is approaching the tip apex towards the surface and looking for the well-known jump to contact phenomenon. Jumps

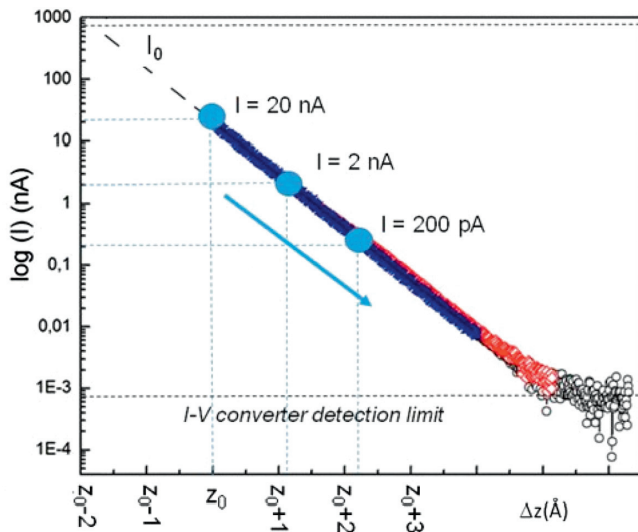


Fig. 6. Three I - Z curves recorded on PS1 in a retraction mode for a 10 mV bias voltage and 3 feedback loop set up currents: 20 nA (blue), 2 nA (red) and 200 pA (black). Those I - Z curves develop between the I_0 single atom contact limit $I_0 = G_0V$ for $V = 10$ mV and the 0.9 pA detection limit of the I - V converter used for PS2. More than 6 orders of magnitude in Z are accessible for this electronic. For the 3 I - Z curves, the extracted apparent barrier height is 3.43 eV \pm 0.2 eV.

to contact between a metallic tip and a metal surface were first recorded in 1987 by Gimzewski and Moller [31] and had continued to be explored over the years [32,33]. A vacuum tunneling junction between a metallic tip apex and a metallic surface has generally a good probability to break down when the tip apex end atom distance to the surface is below $Z = 3$ Å (atom to atom). Below this distance, the conductance can increase very fast due to the attractive adhesive force between the tip apex end atoms and the metallic surface until a metallic nanoscale neck is created between the two [32,33]. During this jump to contact (normally easily observed by a very abrupt junction conductance increase on the I - Z characteristics), a metallic point contact is created between the tip and the sample. Its conductance depends on the precise atomic scale structure of the neck i.e., on the type of metallic surface and on the tip end apex atomic structure.

On the Au(111) surface and as presented in Figure 7, we have reproduced this jump to contact phenomenon with our LT-UHV 4-STM. As compared to the Figure 6 initial feedback loop step up conditions, an intermediate 5 mV bias voltage for a 1 nA feedback tunneling current intensity was used on PS1. Starting from this set up point S and with a 45° oriented tip, the feedback loop was switched off and Z reduced continuously down to 2 Å. As reported in Figure 7, the jump to contact occurs 1.2 Å below S at point J. After this J jump, it reaches a plateau when the metallic atomic neck is formed to the complete contact point. During the tip retraction phase, retardation adhesive forces keep the conductance decreasing slowly forming a small hysteresis cycle as expected [32,33] up to the K breaking point of the neck occurring $\Delta Z = 30$ pm

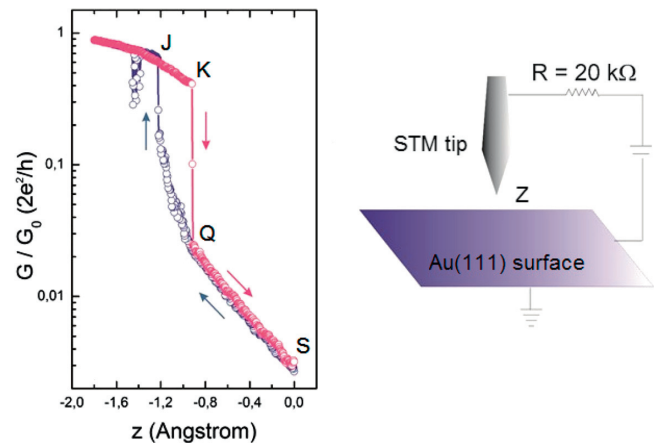


Fig. 7. (a) A complete jump to contact and retraction I - Z characteristics on an Au(111) surface using a gold coated tungsten tip. The initial Z starting point marked S is corresponding to a 5 mV bias voltage and 1 nA feedback current. The S-Q-J curve is the jump to contact characteristics and the K-Q-S curve is the retraction curve. This was recorded on PS1 in a single down and up continuous Z variations forming a nice small loop hysteresis Q-J-K-Q due to the atomic scale mechanic difference between forming and breaking a conductive neck. The awaited G_0 conductance plateau for a single metal atom contact is starting at J on the jump to contact to saturate towards a $0.9 G_0$ contact conductance, a little lower than G_0 . The same conductance plateau is recovered again during the tip retraction up to the K breaking point. The same S set point is recovered after the complete retraction from Q to S indicating that the Au(111) surface remained intact after this rather soft contact. On the S-Q and Q-S portion of those curves, the apparent tunnel barrier work function is 4.2 eV. (b) The schematic of the tunneling junction used for the jump to contact experiment showing the 20 kΩ resistance introduced between the tip and the I - V converter on PS1 to protect the I - V converter input stage in case of a very large current intensity during a large jump to contact.

away from the J point. After the breaking of this metallic neck, a standard I - Z retraction curve is recovered between Q and S reaching again the same S feedback set point than before starting the approach. From Q to S, a vacuum tunneling junction is formed again and the apparent barrier height for this junction is 4.2 eV, a little bit larger than the one found above on the I - Z retraction characteristics Figure 6. The junction conductance plateau after the K point is converging towards $0.9 G_0$ taking into account the 20 kΩ series resistance inserted in the circuit to protect the I - V converter during those measurements.

6 I - V curves of a single atom contact

Beneficiating from the high stability and low noise of our LT-UHV4-STM scanners, we went a step further by recording the I - V characteristics of a single Au ad-atom tunnel junction exactly at electronic contact with this Au ad-atom. This electronic contact point was determined by reaching the maximum current intensity through the

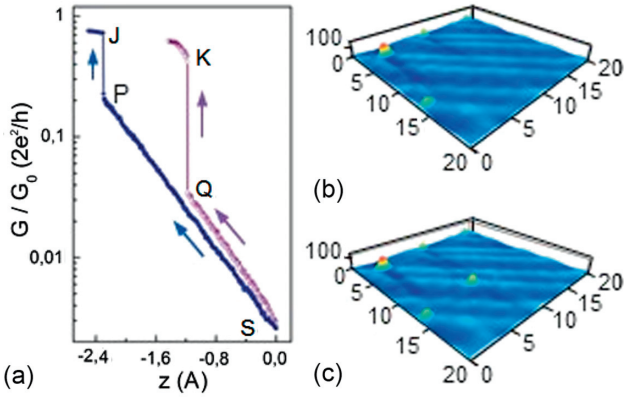


Fig. 8. (a) Two jump to contact characteristics on an Au(111) surface using a gold coated tungsten tip with no retraction curve shown. The initial Z starting point marked S is corresponding to a 5 mV bias voltage for 1 nA feedback current. The first S-P-J approach curve was recorded on a native Au(111) surface on an area corresponding to the STM image (b). After the tip retraction and returning to a standard STM image mode leads to the STM image (c) showing one Au ad-atom more added at the exact position of jump to contact experiment. Starting from the same feedback conditions at S than the S-P-J previous curve, the second S-Q-K approach curve was recorded with the STM tip apex end atom now exactly positioned atop the new Au ad-atom identified in (c). The awaited G_0 conductance plateau for a single metal atom contact is starting at J on the jump to contact to saturate towards a $0.8 G_0$. The (b) and (c) STM images were recorded in a constant current mode for $I = 1$ nA and a 10 mV bias voltage. Image scale $20 \text{ nm} \times 20 \text{ nm}$ for a $100 \text{ pm} \Delta Z$ corrugation. All the measurement were performed here on PS1.

junction but with a minimum mechanical deformation of this junction at contact with the Au ad-atom as previously practiced on a single C_{60} molecule [8]. For this purpose, a single Au ad-atom was first created on Au(111) because using a tip apex coated with Au(111) surface atoms, some very soft jumps to contact events can lead to the transfer of only one Au atom from tip apex to the surface when retracting the tip after a jump to contact [32,33]. This is not observed for all the jump to contact experiments. But when occurring for example during a Figure 8a S-P-J like approach sequence, the surface STM image presented in Figure 8b is showing a new Au ad-atom after the tip retraction at the location of the contact. This image can be compared with the STM image at the same surface location before the S-P-J jump to contact [32,33]. During this S-P-J approach presented in Figure 8a and before the jump to contact at P, the apparent tunneling barrier height calculated from S to P is 5 eV, very close in this case to the 5.4 eV Au(111) work function.

Having located the deposited Au ad-atom on the Au(111) surface (Fig. 8c), the tip apex was positioned atop this ad-atom. Then, two very low voltage I - V characteristics (from -2 mV to $+2$ mV) were recorded after switching off the feedback loop and selecting first 2 very characteristic feedback loop set point currents: $I = 8$ nA and $I = 120$ nA. For a 5 mV bias voltage and on the

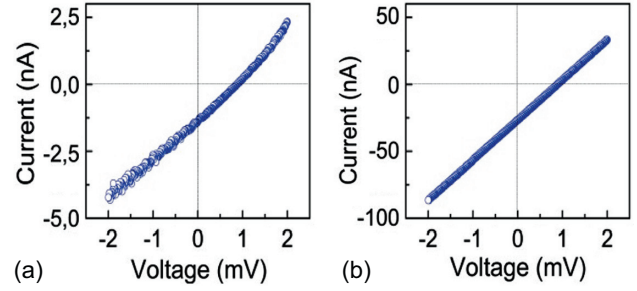


Fig. 9. Two non-averaged very low voltage I - V characteristics recorded (a) for $I = 8$ nA feedback current intensity and a 5 mV Bias voltage and (b) for $I = 120$ nA with also a 5 mV bias voltage with the tip apex end atom exactly positioned atop the Au ad-atom imaged in Figure 8c. $I = 120$ nA is the last stable possible recorded I - V curve before a jump to contact to occur. It was determined by following in real time the $I(t)$ noise on an oscilloscope. Both I - V curves are showing a 1 mV offset voltage attributed to the I - V converter used in those experiments on PS1. The 8 nA set up I - V is not fully linear. This can be attributed to the electronic asymmetry of the “metal tip – vacuum-Au ad-atom-Au(111) surface” tunnel junction where for a 8 nA feedback current, the Au ad-atom is more electronically coupled to the Au(111) surface than to the metallic tip apex end Au atom. The 120 nA I - V characteristics is fully linear and symmetric because of the almost perfect equilibration of the electronic interactions (the Au(111) surface one side and the end atom tip apex on the other side) in the junction before the jump to contact. This is confirmed by the 13 k Ω resistance of this junction instead of the 12.91 k Ω awaited quantum resistance for a one quantum channel of conduction through a single Au ad-atom.

Figure 8a S-P-J jump to contact I - Z characteristics, this corresponds to junction conductance of $0.0206 G_0$ and $0.3100 G_0$ respectively. On the S-P-J Figure 8a I - Z characteristics, this $0.0206 G_0$ conductance set point is positioned in between S and P i.e., before the jump to contact. The $0.3100 G_0$ set point is located in between P and J i.e., in the Figure 8a Z transition values during a jump to contact.

For the $0.0206 G_0$ conductance set point, the I - V presented in Figure 9a is characteristics of a vacuum tunneling junction between the gold end apex of the tungsten tip and the new Au ad-atom deposited on Au(111) by the jump to contact. It was quite stable and do not required any care nor any averaging over a series of I - V curves. As compared to the $0.0206 G_0$ set up conductance, the junction resistance extracted from this almost linear I - V curve is 645 k Ω i.e., $0.0201 G_0$.

For the $0.3100 G_0$ conductance set point, the I - V characteristic was more delicate to record since positioned in the rather unstable jump to contact Z values between P and J. Therefore, contacting the Au ad-atom was performed by approaching the tip apex to surface not continuously as in Figure 8a (or Fig. 7) but by increasing manually the feedback current step by step taking care at each step to avoid any P to J like jump to contact between the tip apex and the Au(111) surface. We were guided for this by the real time the $I(t)$ tunneling current fluctuation

after each increase of the feedback current intensity. Just before any jump to contact, there must be a signature noise increasing in the tunneling current intensity and indicating that the ad-atom is hesitating between surface and tip apex adsorption. Those $I(t)$ variations were followed in direct for each set up current from 8 nA up to 120 nA where the $I(t)$ noise suddenly started to increase. This was the only way to capture the last stable Z value before a real jump to contact. Such an $I(t)$ procedure was effective because of the exceptional stability in Z of our LT-UHV 4-STM scanners (2 pm noise in Z measured in the imaging mode). The Figure 9b $I-V$ curve is very stable for the 120 nA set up point and do not required any averaging over a series of $I-V$ curves. As compared to the $0.3100 G_0$ set up conductance, the junction resistance extracted from this Figure 9b $I-V$ curve is 33 k Ω i.e., $0.303 G_0$. Subtracting the 20 k Ω protection resistance maintained in series in the circuit (see Fig. 6b) from this measured 33 k Ω , the “tip apex-Au ad-atom-Au(111) surface” junction resistance is 13 k Ω . This is very close to the 12.91 k Ω quantum resistance of single atom point contact junction for a single ballistic channel Au atom and the “one shot” Figure 9b $I-V$ characteristic is truly linear at low voltage.

Very indicative of the stability of the LT-UHV 4-STM scanners and after recording the two Figure 9 $I-V$ characteristics, a new jump to contact $I-Z$ characteristics was recorded on this Au ad-atom starting from the same initial S set point (1 nA, 5 mV) i.e., with a Z value larger as compared to the initial $I-Z$ curve because of the supplementary Au atom under the tip apex on PS1. Interestingly and as presented in Figure 8a, the S-Q-K jump to contact on this $I-V$ measured single Au atom occurs at a point Q corresponding to a $0.031 G_0$ and the stability plateau of the metallic contact formed occurs at point K corresponding to a $0.42 G_0$. Therefore, the first 8 nA $I-V$ curve Figure 9a was recorded just before the jump to contact Z values. The 120 nA one Figure 9b was recorded just before the formation of the neck that is just before the mechanical deformation of the “tip apex-Au ad-atom-Au(111) surface” junction leading to a jump to contact. Notice that starting from the same S point, the S-Q-K jump to contact curve is shifted to the right by 1.1 Å as compared to the S-P-J one. This is about the STM corrugation of the Au single adsorbate recorded at the feedback set point S (see Fig. 11).

7 Single atom lateral manipulation

As re-demonstrated in the previous section, some jumps to contact are able to produce single Au ad-atom on Au(111). But to demonstrate the atomic scale writing ability of our LT-UHV 4-STM scanners, more than a few Au ad-atoms are required on the Au(111) surface. Therefore and for testing atom by atom lateral manipulation, individual Au atoms were produced massively on the Au(111) surface following the usual single tip LT-UHV-STM procedure [34]:

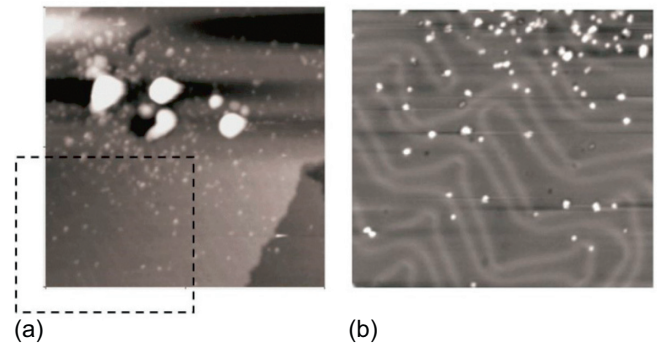


Fig. 10. (a) Constant current STM image of the Au nanoclusters area after its negative pulse destruction showing all the small and large Au adsorbates plus the central crater in the Au(111) surface (recorded on PS3, $I = 200$ pA, $V = 500$ mV, image size 100 nm \times 100 nm). (b) constant current STM image on a flat Au(111) terrace where the herringbone reconstruction are clearly together with about 30 Au ad-atoms, 10 Au dimers and a few other adsorbates composed of more than 2 Au atoms (recorded on PS3, $I = 200$ pA, $V = 500$ mV, image size 50 nm \times 50 nm).

1. an electrochemically etched tungsten tip is indented into the Au(111) surface by more than 1 nm with positive bias voltage higher than 5 V. As a consequence, the end apex of this tip is heavy coated with Au atom,
2. the tip is moved away from the indented Au(111) surface towards a large flat and atomically clean Au(111) terrace (see for example Fig. 2),
3. applying now a negative bias voltage between -3 to -4 V and approaching the gold coated tip apex by 0.8–1.0 nm towards the Au(111) surface leads the tip to release on this surface a few large Au nanoclusters with a diameter generally larger than 10 nm,
4. the tip apex is moved on a given Au nanocluster, is approached by 1.2 nm under now a large positive bias voltage from $+4$ to $+6$ V. As a consequence, this Au nanocluster is normally decomposed in a multitude of very small Au entities and a lot of individual Au ad-atoms can be found around on the Au(111) surface.

As presented in Figure 10a, this process was performed on our LT-UHV 4-STM using PS3 but with a vertical oriented tip. A zoom-in STM image of the random distribution of those Au ad-atoms on the Au(111) surface is also presented in Figure 10b. These scattered Au ad-atoms are now ready to be used for STM single atom manipulations and to construct atomic scale nanostructure by repositioning the atoms one by one on the Au(111) surface as usually practiced with a single tip LT-UHV-STM. Notice that with a 45° tip on PS3, it was very difficult to control a single atom lateral manipulation as compared to the 90° oriented relative to the surface tip used on single tip LT-UHV-STM. With such a 45° tip, the probability of a successful single atom lateral manipulation was less than 10%. On our system and to reach a 70% rate of success comparable to a single tip LT-UHV-STM, the tip holders were modified by rotating the tip holder

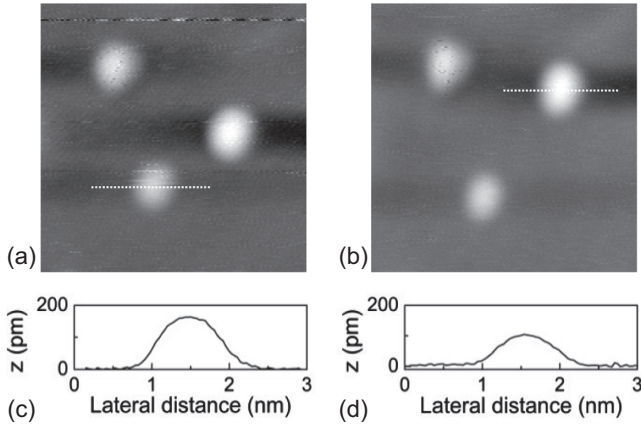


Fig. 11. (a) Constant current STM image of a small $7 \text{ nm} \times 7 \text{ nm}$ Au(111) surface area with 3 adsorbates: two Au ad-atoms and one Au dimers identified using the line scans presented respectively in (c) and (d). The Au dimer was on purpose manipulated from position A to the pre-determined position B in a pushing constant current manipulation mode. (b) Constant current STM image of the same Au(111) surface after the Au dimer manipulation. Both images were recorded on PS3, $I = 20 \text{ pA}$, $V = 500 \text{ mV}$. The tunnel junction resistance during the Au dimer pushing was set up at $500 \text{ k}\Omega$.

micro-tube towards a vertical orientation. In this case, the above described multiple Au ad-atom production can proceed as usual together with single Au atom lateral manipulation. Of course, one inconvenient of this new 90° tip orientation on our LT-UHV 4-STM is that the top navigation UHV SEM cannot image the end apex of 90° oriented tip. This may encourage LT-UHV 4-STM designers to develop a new LT-UHV N-STM version with $N > 4$ scanners where some scanners will be equipped with 90° tip holders for in parallel atom by atom manipulation and the other scanners for atomic scale measurement with a 45° tip holder orientation. This is for example an urgent demand for 4 probes atomic scale electrical measurement along an atomic scale dangling bond wire where a supplementary scanner will be in charge of holding the 90° oriented tip for single H atoms extraction on Si(100)H.

During a lateral single atom manipulation on a surface, the manipulation is controlled by the tip to surface tunneling junction resistance. Generally for a single Au atom manipulation on an Au(111) surface and using a single tip LT-UHV-STM, a junction resistance between $150 \text{ k}\Omega$ and $500 \text{ k}\Omega$ is used in a constant current mode of operation i.e., with the feedback loop ON during the atom manipulation sequence [35]. In this case and when an atom lateral manipulation proceed along the surface, the ΔZ tip apex relative height variations during the manipulation (the so-called manipulation curve [36]) can be recorded in time. It provides very important information on the mechanical behavior of the adsorbate between the tip apex and the surface during the manipulation. Here, the pulling, sliding and pushing modes of lateral manipulation have been observed for a single metallic ad-atom manipulation on a metallic surface [34, 37].

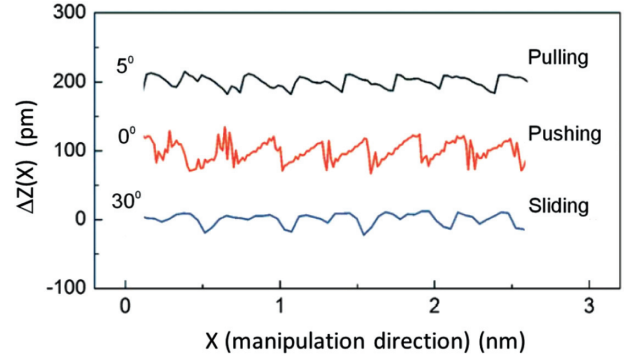


Fig. 12. Contact current manipulation curves on a single Au ad-atom on an Au(111) ultra clean terrace for 3 different tunneling junction resistance R . (i) $R = 330 \text{ k}\Omega$ for a pulling mode. Here, the irregular feature recorded at the beginning (left) of the manipulation signal is caused by a 5° deviation of the manipulation direction relative to the $[110]$ direction on the Au(111) surface [34], (ii) $R = 333 \text{ k}\Omega$ for a pushing mode with no apparent misalignment in this case because of the repulsive force of the tip apex and the Au ad-atom and (iii) $R = 500 \text{ k}\Omega$ for a quasi-sliding mode where the tip apex is supposed to be always atop the Au ad-atom during the manipulation sequence. Here, the misalignment was about 30° according to [34]. For those 3 resistances, the bias voltage was always maintained to 500 mV . The $\Delta Z(t)$ are represented here parameterized by the $X(t)$ tip apex scanning motion leading the presented $\Delta Z(X)$ manipulation curves.

To reproduce those characteristic manipulation curves on our LT-UHV 4-STM, PS3 was equipped with a 90° oriented tip holder, the tip apex was gently indented in the Au(111) surface and was moved at the location of some isolated Au ad-atom monomer and dimer among the many produced on the Au(111) surface. The PS3 STM feedback loop was tuned to reach the standard $150\text{--}500 \text{ k}\Omega$ junction resistances used on LT-UHV-STM for single atom manipulations. For reference and in comparison with what was discussed in Sections 4 and 5, such a junction resistance tuning corresponds to a tip apex end atom to Au ad-atom distance $1\text{--}3 \text{ \AA}$ away from the jump to contact point. Then, the tip was line-scanned in a constant current mode along a selected direction of manipulation. The time dependent $\Delta Z(t)$ tip height variation for PS3 was recorded at the same time leading to the manipulation signal. Before and after a manipulation sequence, STM imaging was performed with the same PS3 to confirm the lateral displacement of the selected Au ad-atoms. Figure 11 is presenting the manipulation of an Au dimers from A to B on the Au(111) surface over a distance of 1.17 nm . This dimer was selected because it was located nearby two single Au ad-atoms. Notice that their position was not perturbed by the manipulation of the dimer in a pushing mode. This was possible because of the 90° tip orientation used in this manipulation. A 45° tip will have also perturbed the other atoms around by its facets.

Obtained during the lateral manipulation of a single Au ad-atom on an Au(111) atomically flat terrace, the pulling (i), pushing (ii) and quasi-sliding (iii) manipulation signals are presented in Figure 12. They were

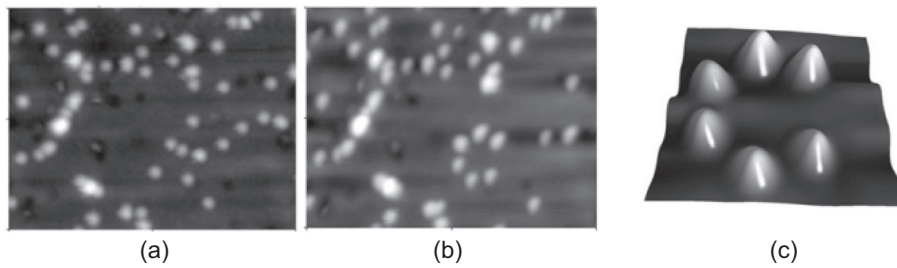


Fig. 13. (a) and (b) constant current STM images of a $20 \text{ nm} \times 16 \text{ nm}$ Au(111) surface where many single Au ad-atom have been manipulated in a constant current pushing mode to construct a letter C with 6 Au ad-atoms. A total of 11 Au ad-atoms have been manipulated 6 for the C and 5 to clean the surface around the C. (c) a pseudo $5.12 \text{ nm} \times 5.12 \text{ nm}$ 3D STM image with $\Delta Z = 0.12 \text{ nm}$ of the central part of the image (b) showing the details of the C letter constructed over an herringbone reconstruction. Both (a) and (b) images were recorded on PS3, $I = 50 \text{ pA}$, $V = 500 \text{ mV}$. The tunnel junction resistance for all the Au ad-atom manipulations was set up at $333 \text{ k}\Omega$.

obtained by selecting respectively three different junction resistance: $150 \text{ k}\Omega$, $330 \text{ k}\Omega$ and $500 \text{ k}\Omega$. For recording very pure manipulation signals, it is very important to use an atomically flat surface [34,37] since any atomic scale corrugation will be reported in the tunneling current and therefore on $\Delta Z(t)$. This is what we have also observed here since on a reconstructed Au(111) surface, any misalignment of the manipulation direction relative to the herringbone orientation leads to irregular and not periodic $\Delta Z(t)$ manipulation signals. This is the explanation why the sliding manipulation signal presented in Figure 12 is not perfect as compared to the one already recorded in the past using a single tip LT-UHV-STM. On a positive side, this confirms that each scanner of our LT-UHV 4-STM is a very performant LT-UHV-STM also in the X and Y lateral directions.

To confirm that any scanner of our LT-UHV 4-STM can construct a surface nanostructure atom by atom, a quite large Au(111) flat terrace was selected and imaged using PS3 to locate a large number of Au ad-atoms produced as explained above (Fig. 13a). As presented in Figure 13, step by step and in a pushing mode, 6 Au ad-atom were manipulated using PS3 to construct the letter C (the first letter of CNRS and of our laboratory CEMES). Per scanner, this demonstrates the nice writing ability of our LT-UHV 4-STM. Some Au ad-atoms were also pushed away from the scene to clean the selected Au(111) terrace. To conclude this section, a nice zoom-in pseudo 3D STM image of this letter is presented in Figure 13c.

8 Two tip Au(111) surface conductance measurements

The atomic resolution STM images presented in Figure 4 were obtained scanner per scanner independently and with a common ground. Taking the advantage of such high performance of our LT-UHV 4-STM, it was also important to demonstrate how to proceed with 2 tips interdependent measurements at the atomic scale. We will describe here only one set of experimental data in this direction. The results presented below open the way for an atomic scale

generalization of the 2 probes I - V measurement performed recently on the MoS₂ surface with an inter-tip distance around 100 nm [15]. Those 2 probes I - V measurements were recorded on a first generation 4 probes machine with no atomic resolution ability per scanner [25].

At first, we show how the high resolution STM imaging performance of the LT-UHV 4-STM is preserved when the Au(111) surface is imaged using two scanners simultaneously operating at the inter-tip distance well below $1 \mu\text{m}$. The tips used in this experiment were mounted on the 45° oriented tip holders on PS2 (tip B) and PS4 (tip C) scanners. Before the experiment, each tip apex was prepared independently by the procedure described above in Section 2 with a very large $100 \mu\text{m}$ separation distance. Then, those tips were progressively navigated to reduce their inter-tip distance by using the top-view UHV-SEM of our LT-UHV 4-STM. The UHV-SEM navigation enables to reduce the inter-tip distance to about 200 nm as presented in Figure 14a. Since the planarity of the gold sample is not mastered on the long range with a nanometer precision during its mounting on the sample stage, the controlled approach was then performed by using the STM feedback loop for each scanner. In this way, we avoided any tip crash in lateral (between two tips) and in vertical (between each tip and the surface) directions. After the gentle approach at the tip separation distance of about 200 nm , these two tips were scanned simultaneously on Au(111) in a constant current mode. The corresponding STM images are presented in Figures 14b and 14c for tip B and tip C, respectively. Tip B was scanned on $5 \text{ nm} \times 5 \text{ nm}$ surface area keeping continuously the atomic resolution (Fig. 14b). At the same time, tip C was scanned larger on a $150 \text{ nm} \times 150 \text{ nm}$ surface area with satisfying performance, i.e., we can clearly observed the Au(111) herringbone reconstruction and the sharp monoatomic step as well. Interestingly, we were also able to collect SEM images of both tips (Fig. 14a), which were approached to the gold sample (their corresponding STM feedback loops were closed). Please notice that in this case, it was necessary to perform the SEM imaging with a low current density (200 pA) in order to avoid any tip crash because of the e-beam capture by the tip. During SEM imaging, the PS2 scanning was stopped. However PS4 was maintained in its

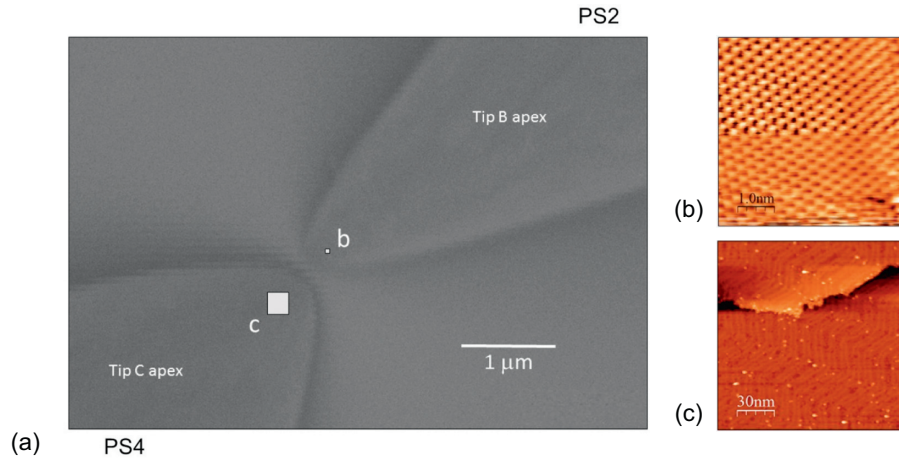


Fig. 14. (a) Top view UHV-SEM image of the 2 tip tunneling junction on the Au(111) surface (10 keV, 200 pA) certifying the 200 nm top tip B to tip C selected distance. Tip apex B is a bit sharper than tip apex C. The small b and large c white superimposed squares on (a) are indicating the STM scanning range for images (b) and (c). (b) PS2 STM constant current image of the Au(111) surface with tip B (1 nA, 10 mV) for a small 5 nm × 5 nm scanning range. (c) STM PS4 constant current image of the Au(111) surface with tip C (0.1 nA, 100 mV) for a large 150 nm × 150 nm scanning range. Images (b) and (c) were recorded simultaneously using the common sample stage ground for both electronics.

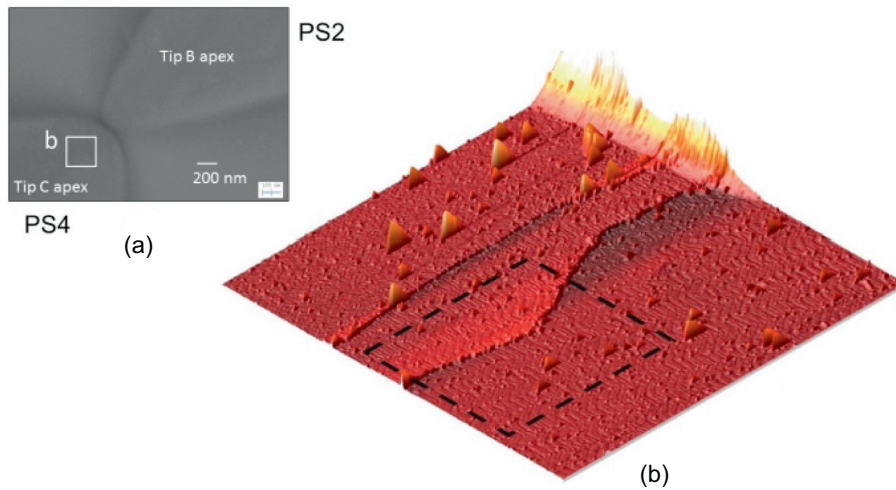


Fig. 15. (a) Top view UHV-SEM image of the 2 tips tunneling junction on the Au(111) surface (10 keV, 200 pA) certifying a 40 nm top tip B to tip C selected distance. The white open square superimposed on (a) is indicating the STM scanning range for the image (b). (b) Pseudo 3D STM constant current image obtained when tip C mounted on PS4 is imaging the surface delimited by the white border square on (a). At the top right part of this STM image, the yellow corrugation is indicating the starting of tip B being scanned by tip C while tip C is benefiting from its feedback loop (0.1 nA, 100 mV, 330 nm × 330 nm). Marked by the dotted black square on (b), the scanning area corresponding to the STM image presented in Figure 14c.

STM scanning mode of operation. This reflects in the little horizontal strips around the SEM image at the end of tip C. Finally, notice that due to the 45° tip orientation with respect to the surface plane, the Figure 14a top-view SEM image does not give access to the exact position of the tip apices providing the STM images. Indeed, the tip terminal gold nanoclusters responsible for the Au(111) surface STM images presented in Figures 14b and 14c are located under the top-view SEM image of the tips, as schematically depicted in the Figure 14a by two white squares.

As presented in Figure 15, we went a step further by reducing again the inter-tip distance. Firstly, we reached

a 40 nm distance (according to the top-view SEM image Fig. 15a). Then, we completely stopped PS2 scanning but maintained its feedback loop active. Secondly, we progressively enlarged the imaging area of tip C mounted on PS4 to finally obtain the STM image of the end of tip B mounted on PS2 using the end apex of tip C as presented in Figure 15b. Note that at the contact between tip B and tip C, the constant current STM image (Fig. 15b) is a composite image resulting from three tunneling current paths to the sample stage ground: (1) the path from the bottom end apex of tip C facing down the Au(111) surface, (2) the lateral path between tip C apex and tip B apex in a

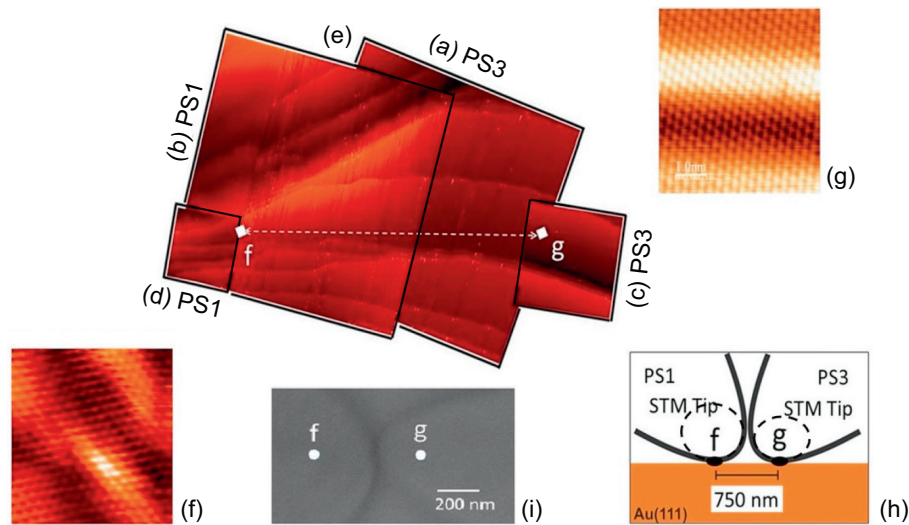


Fig. 16. (e) A mosaic of 4 superimposed constant current STM images (a–d) recorded by PS3 and PS1 and delimited by the white dotted lines on this mosaic. The superposition of those images leads to the determination of the exact distance between the two f and g gold nanoclusters, which were responsible for the atomic-resolution STM imaging of the Au(111) surface performed simultaneously by the use of PS1 (f) and PS3 (g). The scanned area of those STM images are indicated by the small white square on (e). Corresponding STM scanning parameters were (0.1 nA, 1 V, 5 nm × 5 nm) for (f) and (0.5 nA, 100 mV, 5 nm × 5 nm) for (g). (h) A schematic representation of the cross-section of this 2 tip tunneling junction on the Au(111) surface, where the two tip apex radius of curvature is indicated together with the relative position of the (f) and (g) gold nanoclusters facing the Au(111) surface during the simultaneous STM measurements (note 45° tips orientation). The measured distance between (f) and (g) is 750 nm. (i) UHV-SEM (10 keV, 200 pA) top view image of the 2 tip tunneling junction on the Au(111) surface obtained for PS1 and PS3, which were in positions corresponding to STM scanning areas from images (f) and (g), respectively.

lateral contact and (3) the path between the bottom end apex of tip B facing also down the Au(111) surface. As a consequence, the very fast ΔZ corrugation increase back right of the STM image in Figure 15b does not provide any measurement of the distance between the nanoclusters facing the Au(111) surface on both tips, which are the exact STM imaging tip apices. As mentioned above, it is related to the 45° orientation of those tips. Finally notice in Figure 15b the perfectly resolved herringbone reconstruction of the Au(111) surface obtained by scanning with tip C even at about 40 nm distance from tip B.

The determination of the distance between the nanocluster apices of two STM tips is a very important information for any future 2 tips atomic scale electronic contact measurements on a surface. In order to obtain this information for tip B and tip C, the native morphology of atomic steps on our Au(111) surface was used. The atomic step structure of the same surface area was imaged using sequentially tip B and tip C. Then, the respective STM images were overlapped. This procedure leads to a mosaic of constant current STM images presented in Figure 16e. From such a mosaic, the distance between the two STM imaging tip apices f and g can be determined with a precision of a few nanometers. For example, this procedure was applied to the atomic resolution STM images obtained by simultaneous scanning with tip B and tip C (Figs. 16f and 16g). In this case, the relative distance between those tip apices is about 750 nm. Moreover, we also obtained the corresponding top SEM image of both tips in these defined positions on the Au(111)

surface (Fig. 16i). By superimposing all the information, the exact tip apex positions can be determined also on the SEM image. The schematic drawing of the cross-section of this double tip apex tunnel junction (with two respective f and g nanocluster tip apices) is given in Figure 16h. As schematically presented one can take into account the top-view radius of curvature for each tip, which are obtained from SEM image with a precision of 10 to 20 nm (the precision of our UHV-SEM), and correlate them with the tip to tip separation. This methodology for the determination of inter tip apex distance providing the STM images is extremely important for atomic scale electronic contacts. We also point out that this methodology gains from the advantage of having all STM scanners able to image a surface with an atomic resolution. Particularly this crucial feature was missing in the previous version of the 4-probes [25].

The same methodology of tip apex distance determination was applied for dI/dV spectra measurements performed on the Au(111) surface in between 2 STM tips. The energy location of Au(111) surface states relative to the Fermi level is well known [38,39]. They are generally single tip LT-UHV-STM characterized by recording dI/dV tunneling spectra with either tip or sample grounded. Typically a lock-in technique is used to record the dI/dV signal derivative. For the Au(111) surface, the surface states maximum is showing up around -400 mV [38,39]. In our experimental setup, a lock-in electronics with a 500 Hz frequency and a 50 mV modulation amplitude was coupled to the PS4 STM electronic circuitry in

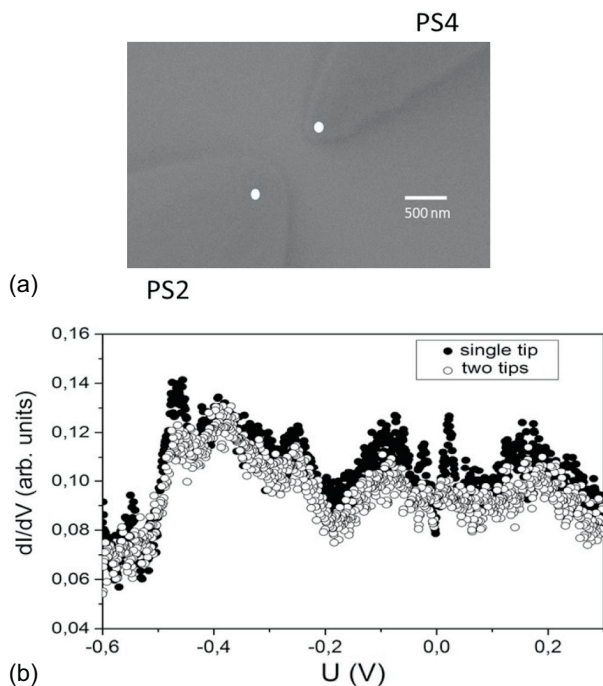


Fig. 17. (a) Top UHV-SEM image (10 keV, 200 pA) of the 2 tip tunneling junction set up on the Au(111) surface to record a floating surface dI/dV spectrum. The PS2 tip was electrically connected to a lock-in electronic system (500 Hz, 50 mV). (b) dI/dV spectra obtained for the Au(111) surface. The first dI/dV spectrum (“single tip”) was recorded with the Au(111) sample stage grounded. It shows the standard dI/dV maximum of the surface states around -400 mV [38,39]. The second superimposed dI/dV spectrum (“two tips”) was recorded with the sample stage ground electronically disconnected. In this case the PS4 tip was used as a ground counter electrode with a defined 10.5 M Ω resistance of the corresponding tunneling junction. For both spectra, the PS2 tip – sample distance was defined by $I = 0.1$ nA and $V = 300$ mV STM feedback loop parameters. The distance between two tip apex gold nanoclusters responsible for the corresponding tip – sample tunneling junctions was estimated to be 1.2 μm as indicated by the white dots in (a) (note that the corresponding tip apex to tip apex distance observed in top SEM image is about 500 nm).

a standard manner [39]. Then, two kind of dI/dV spectra were recorded on Au(111) using our LT-UHV 4-STM. In the first case, we performed a standard, single tip LT-UHV-STM dI/dV experiment, in which the LT-UHV 4-STM sample stage was grounded. In the second case, the sample stage ground was electronically disconnected and we used instead the virtual ground of the PS2 I/V convertor. The tip mounted on PS2 was playing the role of a “top Au(111) surface ground” whose relative distance to the PS4 master tip can be varied within an atomic precision. In our test dI/dV experiment, the distance between the two imaging tip apexes was of about 1.2 μm (Fig. 17a). The two recorded dI/dV spectra are presented in Figure 17b. Each spectrum reproduces nicely the very well-known dI/dV signal for the Au(111) surface state

region [39]. The strong similarity of both recorded spectra can be easily explained by the large inter-tip distance, which exceeds the Au(111) surface 4.3 K electronic mean free path.

9 Conclusions

In this paper, the performances of the new LT-UHV 4-STM stage constructed by ScientaOmicron were explored using an Au(111) surface. We have demonstrated that this new instrument is exactly 4 times a very precise single tip LT-UHV-STM able to scan simultaneously with an inter tip apex distance between 2 front to front tips ranging from millimeters to a few tens of nanometers on the same surface depending of the tip apex end radius of curvature per tip. We have performed large scale constant current imaging of the Au(111) surface, very precise atomic scale imaging using all the 4 scanners independently or in parallel with a ΔZ stability of 2 pm at 4.3 K. For single atom manipulation, we have modified the original tip holder to orient the tip 90° relative to the surface sample. After this transformation, Au atom can be manipulated on the Au(111) surface and the well-known pulling, sliding and pushing manipulation signal were recorded as if those manipulations were performed on a very stable single tip LT-UHV-STM. Jump to contact experiments lead to record the linear $I-V$ characteristics of a single Au ad-atom exactly electronically contacted with no need to average over many such $I-V$ curves at 4.3 K.

We have also started to play with 2 tip surface electronic measurements in a floating mode of operation succeeding for a small tip apex to atomic apex contact surface distance of 1.2 μm to capture dI/dV characteristics usually recorded with one STM tip and with the sample stage connected to the ground while keeping atomic resolution per tip. For two 45° oriented tips and using the top UHV-SEM and STM images, we have also determined the position of the metallic nanocluster facing the surface and responsible for the STM imaging. With this new LT-UHV-4 STM head, we are now entering in a new era of atomic scale measurements for atomic scale wires and circuits, single molecular wires and intramolecular circuits but also for performing single molecule mechanics on atomically loaded single molecule motors and on trains of molecule-gears up to solid state nanoscale gears.

We thank the Midi-Pyrénées “Contrat de Plan Etat Region Campus G. Dupouy” (2007–2014) for the complete financial support for the LT-UHV-4 STM machine and particularly the constant support from the Region Midi-Pyrénées, the Toulouse Metropole, the FEDER and the CNRS. We like also to thank ScientaOmicron for permanent technical supports during this work. This work was supported by the MANA NIMS project and by the European projects AtMol and PAMS. D.S. thanks CEA-Tech for financial support during this work. M.K. acknowledges financial support received from the Polish National Science Centre for preparation of his Ph.D. dissertation (decision number: DEC-2013/08/T/ST3/00047) and from the Foundation for Polish Science (FNP).

References

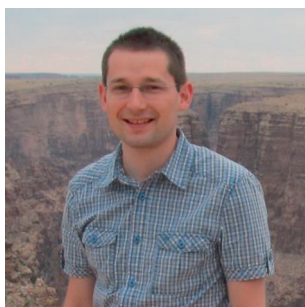
1. C.J. Chen, *Introduction to Scanning Tunneling Microscopy* (Oxford University Press, Oxford, 2008)
2. H.C. Manoharan, C.P. Lutz, D.M. Eigler, *Nature* **403**, 512 (2000)
3. D.M. Eigler, E.K. Schweizer, *Nature* **344**, 524 (1990)
4. G. Meyer, S. Zophel, K.H. Rieder, *Phys. Rev. Lett.* **77**, 2113 (1996)
5. T.A. Jung, R.R. Schlittler, J.K. Gimzewski, H. Tang, C. Joachim, *Science* **271**, 181 (1996)
6. F. Moresco, G. Meyer, K.H. Rieder, H. Tang, A. Gourdon, C. Joachim, *Phys. Rev. Lett.* **87**, 088302 (2001)
7. A. Aviram, C. Joachim, M. Pomerantz, *Chem. Phys. Lett.* **146**, 490 (1987)
8. C. Joachim, J. Gimzewski, R.R. Schlittler, C. Chavy, *Phys. Rev. Lett.* **74**, 2102 (1995)
9. A. Yazdani, D.M. Eigler, N.D. Lang, *Science* **272**, 1921 (1996)
10. V. Langlais, R.R. Schlittler, H. Tang, A. Gourdon, C. Joachim, J.K. Gimzewski, *Phys. Rev. Lett.* **83**, 2809 (1999)
11. L. Lafferentz, F. Ample, H. Yu, S. Hercht, C. Joachim, L. Grill, *Science* **323**, 1193 (2009)
12. C. Toher, R. Temirov, A. Gruling, F. Pump, M. Kaczmarek, G. Cuniberti, M. Rohlfing, F.S. Tautz, *Phys. Rev. B* **83**, 155402 (2011)
13. G. Reece, F. Scheurer, V. Speisser, Y.J. Dappe, F. Mathevet, G. Schull, *Phys. Rev. Lett.* **112**, 047403 (2014)
14. C. Manzano, W.H. Soe, H.S.J. Wong, F. Ample, A. Gourdon, N. Chandrasekhar, C. Joachim, *Nature Mat.* **8**, 576 (2009)
15. R. Thamankar, T.L. Yap, K.E.J. Goh, C. Troadec, C. Joachim, *Appl. Phys. Lett.* **103**, 083106 (2013)
16. M. Kolmer, S. Godlewski, H. Kawai, B. Such, F. Krok, M. Saeys, C. Joachim, M. Szymonski, *Phys. Rev. B* **86**, 125307 (2012)
17. S.R. Schfield, P. Studer, C.F. Hirjibehedin, N.J. Curson, G. Aeppli, D.R. Bowler, *Nature Comm.* **4**, 1649 (2013)
18. M. Kolmer, S. Godlewski, J. Lis, B. Such, L. Kantorovich, M. Szymonski, *Microelectron. Eng.* **109**, 262 (2013)
19. M. Kolmer, S. Godlewski, R. Zuzak, M. Wojtaszek, C. Rauer, A. Thuai, J.M. Hartmann, H. Moriceau, C. Joachim, M. Szymonski, *Appl. Surf. Sci.* **288**, 83 (2014)
20. U.G.E. Perera, F. Ample, H. Kersell, Y. Zhang, G. Vives, J. Echeverria, M. Grisolia, G. Rapenne, C. Joachim, S.-W. Hla, *Nature Nanotechnol.* **8**, 46 (2013)
21. R. Ohmann, J. Meyer, A. Nickel, J. Echevaria, C. Joachim, F. Moresco, G. Cuniberti, *ACS Nano* **9**, 8394 (2015)
22. M. Kolmer, R. Zuzak, S. Godlewski, M. Szymonski, G. Dridi, C. Joachim, *Nanoscale* **7**, 12325 (2015)
23. M. Sakurai, C. Thirstrup, T. Nakayama, M. Aono, *Surf. Sci.* **386**, 154 (1997)
24. T. Nakayama et al., *Adv. Mat.* **24**, 1675 (2012)
25. C. Joachim, D. Martrou, M. Rezeq, C. Troadec, D. Jie, N. Chandrasekhar, S. Gauthier, *J. Phys. Condens. Matter.* **22**, 084025 (2010)
26. *Atomic Scale Interconnection Machines*, Springer Series: Advances in Atom and Single Molecule Machines, edited by C. Joachim, vol. 1 (Springer-Verlag, Berlin, 2012)
27. J. Deng, C. Troadec, H.K. Kim, C. Joachim, *J. Vac. Sci. Tech. B.* **28**, 484 (2010)
28. F. Hanke, J. Björk, *Phys. Rev. B* **87**, 235422 (2013)
29. *Scanning Tunneling Microscopy Vol. I*, edited by H.J. Guntherodt, R. Wiesendanger (Springer-Verlag, Berlin, 1994)
30. G. Binnig, H. Rohrer, C. Gerber, E. Weibel, *Appl. Phys. Lett.* **40**, 178 (1982)
31. J.K. Gimzewski, R. Moller, *Phys. Rev. B* **36**, 1284 (1987)
32. L. Limot, J. Kroger, R. Berndt, A. Garcia-Lekue, W.A. Hofer, *Phys. Rev. Lett.* **94**, 126102 (2005)
33. J. Kroger, H. Jensen, R. Berndt, *New J. Physics* **9**, 153 (2007)
34. S.W. Hla, K.F. Braun, K.H. Rieder, *Phys. Rev. Lett.* **67**, 201402 (2003)
35. L. Bartels, G. Meyer, K.H. Rieder, *Chem. Phys. Lett.* **285**, 284 (1998)
36. X. Bouju, C. Girard, H. Tang, C. Joachim, L. Pizzagalli, *Phys. Rev. B* **55**, 16498 (1997)
37. L. Bartels, G. Meyer, K.H. Rieder, *Phys. Rev. Lett.* **79**, 697 (1997)
38. Ph. Avouris, I.W. Lyo, R.E. Walkup, Y. Hasegawa, *J. Vac. Sci. Tech. B* **12**, 1447 (1994)
39. L. Burgi, H. Brune, K. Kern, *Phys. Rev. Lett.* **89**, 176801 (2002)



Jianshu Yang joined Pico-Lab GNS/CEMES-CNRS in 2012. Her research interest is scanning tunneling microscopy (STM), single atom and molecule manipulations. Dr. Yang got her Ph.D. at Fudan University China in 2001.



Delphine Sordes is a Ph.D. student of the University P. Sabatier Toulouse, detached since November 2013 from CEATech Toulouse to Pico-Lab to work on atom manipulation on the Si(100)H surface for atomic scale surface interconnects using the LT-UHV 4-STM.



Marek Kolmer is a research assistant of the Faculty of Physics, Astronomy and Applied Computer Science at the Jagiellonian University in Krakow (Poland), from where he received his Ph.D. degree in Physics in 2014. His research interests are the fabrication and experimental verification of functional properties of molecular and atomic structures on semiconducting surfaces, i.e., hydrogenated surfaces of silicon and germanium.



David Martrou is 1st Class Charge de Recherche at Pico-Lab working on the field of surface science, MBE growth of large electronic gap surfaces. He is an expert on NC-AFM, KP-AFM and LT-UHV-STM.



Christian Joachim is Directeur de Recherche CNRS at Pico-Lab well known for its seminal work on surface supported single molecule-machine (logic gates, gears, motors). He is an expert of STM measurement of the conductance of a single molecule and on the driving of single molecule mechanical machinery.